

Chapter 5

General conclusions

The mountains have rules. They are harsh rules, but they are there, and if you keep to them you are safe. A mountain is not like men. A mountain is sincere. The weapons to conquer it exist inside you, inside your soul.

Walter Bonatti

Climate change impacts are non uniformly distributed over the globe, with a strong impact on the environment in mountainous areas, especially because mountain ecosystems depend on climatic conditions that vary as a function of altitude. In the recent years, it has become clear that the manifestation of climate change depends on elevation: the measurements so far available in the various mountain regions of the world have confirmed that, on average, mountains are warming more rapidly than surrounding regions. The rate of warming is amplified with elevation, such that high-mountain environments experience more rapid changes in temperature than environments at lower elevations. Significant changes of precipitation are also expected in the changing climate and orographic effects are important in determining the amount of rainfall at a given location. Thus it becomes particularly important to understand how mountains responds to global warming and to anthropogenic forcing.

This dissertation focused on the altitudinal dependencies of meteorological conditions in the Great Alpine Region (GAR), one of the highest and most extensive mountain range system in Europe where both global and local anthropic activities impact it. The Alps serve as a natural barrier, as they surround highly urbanised areas, trapping smog and haze in the valleys of northern Italy. In Chapter 2, observational data over the GAR have been analyzed to study the actual representation of the status of atmospheric variables such as precipitation. Using a large rain gauge dataset,

we showed that the distribution of annual precipitation among the lowlands and the mountains has varied over time, with an increase of the precipitation at the high elevations compared to the low elevations starting in the mid 20 century and peaking in the 1980s. The simultaneous increase and peak of anthropogenic aerosol load is discussed as a possible source for this inter-decadal change. Indeed a varying aerosol concentration has potential impacts on the orographic enhancement of precipitation essentially for two effects: the corresponding change in atmospheric stability and the possible change in the microphysical properties of clouds. At present it is however unclear what process would dominate in determining the response of precipitation to varying aerosol loads, however results seem to indicate that the increased pollution might have increased the orographic enhancement of precipitation, but it is not clear whether this should be related to a suppression of precipitation in the heavily polluted lowlands or an increased precipitation at higher elevations.

With the aim of shedding more light on the aerosols effects at different altitudes, Chapter 3 describes a numerical study over the GAR: using the Weather Research and Forecasting model, the altitude-dependence of the cloud mediated indirect effects of aerosols have been studied over the GAR. Two different 5-years long simulations have been run, differing only in terms of the aerosol load: in the POLLUTED experiment the mean aerosol concentration in the atmospheric boundary layer is on average about one order of magnitude larger than in the PRISTINE simulation in the lowlands, while similar concentrations are found over the mountains. We show that seasonal mean cloud cover, temperature, and precipitations are affected by the aerosol concentrations in the air column, and that the response to pollution is both elevation and season dependent. The overall cloud cover increase with aerosol levels leads to either surface cooling or warming depending on the surface albedo (snow covered or not). Furthermore, different types of clouds have a different sensitivity to aerosols: while the lifetime of low pressure system clouds and orographic clouds is generally increased at high levels of aerosols, convective clouds (typical of the summer season) can actually decrease at high levels of pollution, due to the reduction of strong updrafts.

A third complementing research topic has been tackled in this research project, based on investigating the expected changes in climate over the GAR with a greater emphasis in understanding changes with altitude. In Chapter 4 we investigate predicted changes using the Weather Research and Forecasting Model running 30-year historical simulations (1979-2008) and climate-change projections (2038-2068) at convection permitting resolution (4Km) to be able to better model the interaction between the air masses and the complex orography of this area. This study focused on the altitudinal dependence of historical and future ETCCDI Climate Change indices, showing that different physical processes at different altitudes describe the elevation dependence of temperature and precipitation: both variables are affected by climate change with an altitude dependence changing seasonally.

Among the future developments of this line of research, it is worth mentioning studies varying the concentration of cloud condensation nuclei and ice-nuclei separately to shed light on their relative role in cloud formation, duration, and precipitation; idealized bidimensional and

tridimensional studies to properly account for small-scale processes not considered in this thesis, such as turbulent mixing; studies that analyze also separately aerosol direct and semi-direct effects on radiation, that could modify, even substantially, the climatic response; studies taking into account an ensemble of simulations on the Greater Alpine Region to obtain even more precise quantitative results, and finally studies on precipitation extremes which, however, can evaluate not only on a daily but also on a sub-daily time scale.

This research project demonstrates that the orographic enhancement of precipitation dependence on anthropogenic forcing is an important research line, and in-depth studies are necessary in order to quantify the effects of both aerosols and global warming on it and on other thermodynamic variables. This is an important key point because it will allow us to make more reliable predictions in the mountain regions in the coming decades.

Appendices

Appendix A

The Weather Research and Forecasting (WRF) Model

The Weather Research and Forecasting (WRF) Model is an atmospheric model born in the early 90's from a collaborative effort between the National Center for Atmospheric Research (NCAR), the National Oceanic and Atmospheric Administration, the U.S. Air Force, the Naval Research Laboratory, the University of Oklahoma, and the Federal Aviation Administration (FAA). The goal of the partnership was to design a model useful both for research purposes and for Numerical Weather Prediction (NWP).

The model can be used for a lot of applications, it works from scales of meters to thousands of kilometers. For researchers, WRF can produce simulations based on real atmospheric conditions or idealized conditions offering operational forecasting, and reflecting advances in physics, numerics, and data assimilation contributed by developers from the expansive research community. Indeed WRF Model is a supported “community model”, it has an open-source code in the public domain, and its use is unrestricted, allowing the large worldwide community of registered users to improve the code and the efficiency.

The Dynamical Core usually refers to the Governing Equations and the Numerical Procedure to solve them. NWP models represent the behaviour of the atmosphere which is described by the governing equations. These equations can be derived from various conservation principles and related approximations such as conservation of motion (momentum), conservation of mass, conservation of heat (thermodynamic energy), conservation of water (mixing ratio/ specific humidity) in different forms and conservation of other gaseous and aerosol material. The equations are written in the Eulerian framework in which values and their derivatives are evaluated at fixed locations on the earth.

WRF offers two dynamical cores for its computation of the atmospheric governing equations, and the variants of the model are known as WRF-ARW (Advanced Research WRF) and WRF-NMM

(Nonhydrostatic Mesoscale Model) developed and maintained by the Mesoscale and Microscale Meteorology Division of NCAR. These two dynamical cores include mostly advection, pressure gradients, Coriolis, buoyancy, filters, diffusion, and time-stepping. Physics, the software framework, and parts of data pre- and post-processing are shared between the dynamical cores. The ARW dynamics solver integrates the compressible, nonhydrostatic Euler equations that are cast in flux form using variables that have conservation properties.

WRF Model supports a variety of capabilities:

- fully compressible Euler non hydrostatic equations with hydrostatic option;
- scalar-conserving flux form for prognostic variables;
- complete Coriolis and curvature terms;
- nesting: one-way, two-way with multiple nests, moving nests;
- Mapping to Sphere: 3 map projections are supported for real-data simulations (Curvature terms included);
- Runge-Kutta 2nd and 3rd order time step options;
- 2nd to 6th order advection options (horizontal and vertical);
- positive-definite advection option for moisture, scalar and Turbulent Kinetic Energy;
- time-split small step for acoustic and gravity-wave modes;
- lateral boundary conditions;
- full physics options for land-surface, PBL, radiation, microphysics and cumulus parameterization;

The equations of motion, which form the basis for all NWP models, have their form in pressure coordinates. Pressure coordinate systems are not particularly suited to solving the forecast equations because they can intersect mountains and thus have problems over orographic forecast domain. To address the problem of discontinuous forecast surfaces, the η coordinate was created that is defined as a terrain-following mass vertical coordinate [139]. η is defined as

$$\eta = \frac{p_h - p_{ht}}{p_{hs} - p_{ht}} \quad (\text{A.1})$$

where p_h is the hydrostatic component of the pressure, and p_{hs} and p_{ht} refer to values along the surface and top boundaries, respectively. η varies from a value of 1 at the surface to 0 at the upper boundary of the model domain (Figure A.1).

The η levels allow the bottom atmospheric layer of the model to be represented within each grid box as a flat "step," rather than sloping in steep terrain. They also allow models to have extreme differences in elevation from one grid point to its neighbor, developing strong vertical motions in areas of steep terrain and thus more accurately represent many of the blocking effects that mountains can have on stable air masses. Even when the step-like eta is used as the vertical coordinate, model terrain is still much coarser than real terrain. Although this representation of terrain is a source of error in areas strongly affected by small-scale terrain features, it is still necessary to depict the average elevation within the entire grid box area. Representing terrain in this manner impacts the scale of features that can be preserved in the model's forecast, making the forecast representative of the average conditions in the grid box.

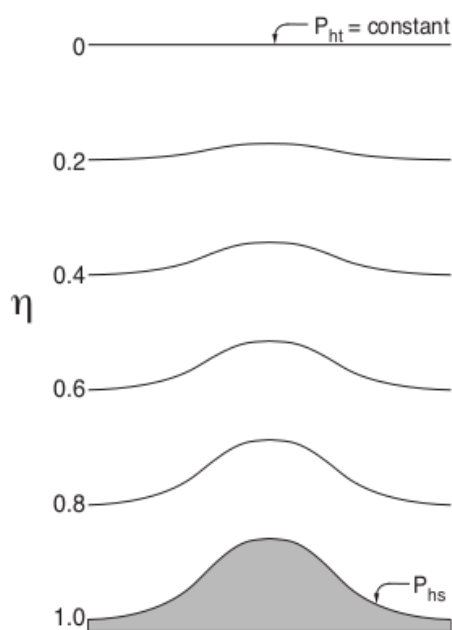


Figure A.1: ARW η coordinates [140]

A.1 Governing equations

The set of the equations used in a NWP model is very large: in this paragraph, the principal equations are described.

The Momentum Equation: the momentum equation is a partial differential equation that describes how the velocity or momentum of a fluid responds to internal and imposed forces. The momentum equation can be stated as:

$$\frac{D\bar{v}}{Dt} = -\frac{1}{\rho}\nabla p - \nu\nabla^2\bar{v} + F_b$$

where \bar{v} is the three-dimensional velocity vector, p is the pressure, ν is the kinematic viscosity and F_b represents external body forces (per unit mass) such as gravity [141]. Equation is called the Navier–Stokes equation.

The horizontal wind is a primary weather variable: the acceleration of the horizontal wind is on the order of 10^{-4} [m/s²] compared with 10^{-7} [m/s²] for the vertical acceleration. Primitive equation models assume that horizontal scales are much larger than vertical scales, which applies to synoptic and planetary circulations, thus the vertical momentum equation is replaced by the hydrostatic approximation, in which the weight of the atmosphere balances the vertical pressure gradient and no vertical accelerations are calculated explicitly. However, the hydrostatic assumption does not hold when the length and depth are similar (typically less than 10 Km). Deep convection, which is common in the tropics, is non-hydrostatic. Therefore, the rate of change of vertical motion is calculated as the sum of the advection, local buoyancy, and non-hydrostatic vertical pressure gradient minus the precipitation drag. These models can reproduce mesoscale convection in realistic detail but they are subject to error in timing and placement of convection. Non-hydrostatic models have the disadvantage of being computationally intensive.

The Continuity Equation: a fundamental principle in meteorology is that mass is conserved except for external sources and sinks, as described by the equation below [141]:

$$\frac{D\rho}{Dt} + \rho\nabla \cdot \bar{v} = 0$$

This form of the equation is useful for forecasting as it relates the rate of density increase, following an air parcel, to the velocity divergence.

The Thermodynamic Equation: this equation describes the conservation of energy applied to a moving fluid element. For a system in thermodynamic equilibrium, the change in internal energy is due to the difference between work done by the system and heat added to the system, written as:

$$c_v \frac{DT}{Dt} + \frac{D\alpha}{Dt} = Q$$

where $c_v \frac{DT}{Dt}$ represents the change in internal energy per unit mass and $\frac{D\alpha}{Dt}$ the rate of work by the fluid system per unit mass. Q is the heating rate.

A.2 Parametrization

NWP models are not able to resolve explicitly those processes which are smaller than the grid scale of the model, thus these processes have to be parameterized. Parameterization means the description of the overall effect of a given subgrid scale process on the grid scale values, using the given grid scale variables.

In this section the main parametrizations used in this thesis are described:

1. The Yonsei University Scheme (YSU) is used for the Planetary Boundary Layer (PBL) because it accurately simulates deeper vertical mixing in buoyancy-driven PBLs with shallower mixing in strong-wind regimes. This scheme proposes a revised vertical diffusion package with a nonlocal turbulent mixing in the PBL that is suitable for weather forecasting and climate models. An explicit treatment of the entrainment processes at the top of PBL is included that produces a realistic structure of the PBL in response to an idealized daytime variation of surface heat and moisture fluxes [107].
2. The radiation schemes provide atmospheric heating due to radiative flux divergence and surface downward longwave and shortwave radiation for the ground heat budget. Longwave radiation includes infrared or thermal radiation absorbed and emitted by gases and surfaces. Upward longwave radiative flux from the ground is determined by the surface emissivity that in turn depends upon land-use type, as well as the ground (skin) temperature. Shortwave radiation includes visible and surrounding wavelengths that make up the solar spectrum. Hence, the only source is the Sun, but processes include absorption, reflection, and scattering in the atmosphere and at surfaces. For shortwave radiation, the upward flux is the reflection due to surface albedo. Within the atmosphere the radiation responds to model-predicted cloud and water vapor distributions, as well as specified carbon dioxide, ozone, and (optionally) trace gas concentrations. The radiative transfer treatment in the Rapid Radiative Transfer Model for GCMs (RRTMG) parameterization is the most complex of all schemes available in the WRF-ARW model and the scheme is described in Iacono et al., 2008 [108]. In this study CAM Green House Gases (GHG) has been used: it provides yearly green house gases from 1765 to 2500. Once the model is compiled, RRTMG long-wave schemes reads these time-varying GHG values from a table (annual global means).
3. The WRF model can make use of several cumulus parameterization schemes, that are useful mainly for the summertime convection: warm-season convective events have been shown to be represented less accurately than cold-season events [142]. This is because of

the large-scale dynamic forcing during the cold-season events that are dominant in winter: they are modeled more accurately than the strong thermal forcing at the surface. The convection parametrization is so necessary to account for the vertical motions not explicitly represented at a coarser resolution. In this thesis the outer domain of the climate and the polluted-pristine simulations include the convection parameterization Tiedtke Scheme [109]: Tiedtke scheme uses the mass-flux approach to represent deep, shallow, and mid-level subgrid convections [109], that is triggered if the parcel's temperature exceeds the environment temperature by a temperature threshold of 0.5°K . This scheme distinguishes penetrative, shallow convection, mid-level convection, and convection starting above the planetary boundary layer.

List of Figures

1.1	<i>Synthesis of trends in mean annual surface air temperature in mountain regions, based on 4672 observation stations (partly overlapping) aggregated in 38 datasets reported in 19 studies. Each line refers to a warming rate from one dataset, calculated over the time period indicated by the extent of the line. Colours indicate mountain region, and line thickness the number of observation stations used. [8]</i>	3
1.2	<i>Glacier mass budgets for eleven mountain regions and these regions combined. Annual and time-averaged mass-budget estimates include the errors reported in each study. Red and blue bars on map refer to regional budgets averaged over the period 2006–2015 in units of $\text{kg}\cdot\text{m}^{-2}\cdot\text{yr}^{-1}$ and mm sea level equivalent (SLE) yr^{-1}, respectively, and are derived from each region’s available mass-balance estimates. [8]</i>	5
1.3	<i>Image taken on December 20, 2003, by the Moderate Resolution Imaging Spectroradiometer (MODIS) on NASA’s Aqua satellite, (https://visibleearth.nasa.gov/images/69816/the-alps)</i>	7
1.4	<i>Schematic diagram showing the various radiative mechanisms associated with cloud effects that have been identified as significant in relation to aerosols. The small black dots represent aerosol particles; the larger open circles cloud droplets. Straight lines represent the incident and reflected solar radiation, and wavy lines represent terrestrial radiation. The filled white circles indicate cloud droplet number concentration. The unperturbed cloud contains larger cloud drops as only natural aerosols are available as cloud condensation nuclei, while the perturbed cloud contains a greater number of smaller cloud drops as both natural and anthropogenic aerosols are available as cloud condensation nuclei. The vertical grey dashes represent rainfall, and LWC refers to the liquid water content. [59]</i>	8

2.1	<i>Topography (upper panel) and annual mean precipitation (1961-1990) at the different rain gauge stations (lower panel) in the Great Alpine Region.</i>	13
2.2	<i>Number of available stations within the Lombardy region for every year in each class of altitude: height more than 1000 m (blue line), more than 400 m (red line) and less than 400 m (black line).</i>	14
2.3	<i>(a) Annual mean precipitation, relative standard deviation (fine error bars) and relative standard error of the mean (bold error bars) for each class of altitude. The full line is the linear interpolation of the points, and it represents the model used to normalize precipitation data for the Lombardy region, according to each station elevation (as described in the Methods). (b) Percentage variation in annual precipitation in the studied 30 year period (1961-1990), for different elevation classes. These variations have been computed from linear trends over the 30 year period. Error bars represent one standard deviation of the percentage variation in annual precipitation calculated on each station.</i>	15
2.4	<i>Seasonal mean precipitation and relative standard deviation for each class of altitude; each panel refers to a different season.</i>	17
2.5	<i>Relative change in seasonal precipitations as function of station elevation, for the period 1961-1990: (a) winter (December, January, February); (b) summer (June, July, August).</i>	18
2.6	<i>Relative change of seasonal precipitation in the GAR over the 1961-1990 period as a function of elevation, for (left panel) spring and (right panel) fall.</i>	18
2.7	<i>(a) Scatter plot of the yearly precipitation averaged over the mountain and lowland stations in the GAR. (b) Scatter plot of the yearly normalized precipitation averaged over the mountain and lowland stations in the Lombardy region. Each point correspond to the values of a given year (in the 1961-1990 period for panel a, and in the 1920-2017 period for panel b). Solid lines show the linear interpolation of the data. In both cases the correlation coefficients between the mountain and lowland annual precipitation time series (equal to 0.9 in both panels) are statistically significant at the 99% confidence level. The colours of the points represent the phase of the NAO of the year to which they refer: positive phase (red), negative phase (blue) and neutral phase (black). The circles represent points whose NAO phase is not available.</i>	19

2.8	<i>Time series of the orographic enhancement of precipitation over the whole GAR (Ro) for the period 1961 to 1990 and over the Lombardy region (OEPI). In the time series of the OEPI over the Lombardy region, dashed lines refer to the period before 1951 in which the low number of stations available makes the series significantly less reliable. The grey band on the time series represents the standard error of the mean for each annual value. A 11-year window, 3-year standard deviation Gaussian filter (black line) is shown with its twice standard deviation on the filter (95% confidence limits), calculated through the propagation of uncertainty. The uncertainty used is the standard error of the mean (grey band on the filter). The trend over the period 1961-1990 (indicated by the thin black line in the lower portion of the figure) is significant at the 99% confidence level and its value is 0.004 yr^{-1}, leading to an increase of the orographic enhancement of precipitation from 1.20 to 1.31 over the 30 year period.</i>	21
2.9	<i>Time series of the orographic enhancement of precipitation over the whole GAR (Ro) for the period 1961 to 1990 and over the Lombardy region (OEPI), analogous to Figure 2.8, but performed for different seasons (extended winter SONDJFMAM, top panel; summer JJA, bottom panel).</i>	22
2.10	<i>Different subregions used in the study: Western Alps (red box), Central Alps (blue box), Eastern Alps (green box), Apennines (yellow box). The thick black lines indicate the Alpine (full line) and Apennines (dashed line) watersheds. Thin black contour lines are lines of constant elevation, drawn from sea level every 500 m.</i>	23
2.11	<i>Annual precipitation as function of elevation in the three Alpine subregions (top panels), the two Alpine watersheds (middle panels) and the two Apennines watersheds (bottom panels). Points indicate the mean value and errorbars indicate the standard deviation computed over the different stations in each class. The total number of station in each subregion is indicated in Table 2.2.</i>	25
2.12	<i>Same as fig. 2.13, bottom panels (the two watersheds of the Apennines), but for winter (DJF) only.</i>	26
2.13	<i>Relative change of annual mean precipitation for the studied 30 year period (1961-1990), for different elevation classes. These variations have been computed from linear trends over the 30 year period. Error bars represent the standard deviation of the percentage variation in seasonal precipitation calculated on each station. Top panel: Alps, partitioned into Western, Central, and Eastern Alps. Middle panel: Alps, partitioned according to the watershed. Bottom panel: Apennines, partitioned according to the watershed.</i>	27

3.1	<i>Topography in the two domains used for the 5-long years runs: bigger domain 12 Km and inner domain 4 Km of resolution.</i>	33
3.2	<i>QNWFA2D variable: surface input flux of water-friendly aerosols.</i>	35
3.3	<i>Seasonal mean concentration of water-friendly aerosols over the PBL.</i>	37
3.4	<i>Daily cycle of PBLH as a function of ground elevation in DJF (a) and JJA (b) for the PRISTINE run. Only land points have been taken into account to make this figure.</i>	38
3.5	<i>Seasonal mean difference in 2 m temperature in Winter (a) and Summer (b). Seasonal relative variation of number of cloud events in DJF (c) and in JJA (d). Coloured pixels represent points that are significant at the 95% confidence level. Altitude isolines are shown every 500 m.</i>	39
3.6	<i>Daily cycle of the difference of the mean hourly temperature at 2 m in DJF (a) and in JJA (b). Daily cycle of the relative variation of the mean hourly number of cloud events in Winter (c) and in Summer (d). Crosses represent points that are not significant at the 95% confidence level.</i>	40
3.7	<i>Relative variation of the number of events with at least 3.5 m/s vertical velocity in function of elevation in JJA. Vertical velocity analysis has been done dividing the data in 18 classes based on station altitude, where the class limits are chosen so that each class has the same number of stations. The mean of each class is calculated and plotted with black dots. Colors represent the density of the points in the GAR from yellow (high density) to blue (low density).</i>	42
3.8	<i>Relative variation of the number of updrafts per each class of daily maximum vertical velocity in JJA, between POLLUTED and PRISTINE runs. Only land points have been taken into account.</i>	42
3.9	<i>Relative variation of the mean seasonal precipitation in function of elevation in DJF (a) and in JJA (b). Precipitation analysis has been done dividing the data in 18 classes based on station altitude, where the class limits are chosen so that each class has the same number of stations. The mean of each class is calculated and plotted with black dots. Colors represent the density of the points in the GAR from yellow (high density) to blue (low density).</i>	43
3.10	<i>Concluding sketch representing the anomaly features in a POLLUTED environment in lowlands and highlands for (a) winter time (DJF) and (b) summer time (JJA). The time is in UTC.</i>	44

3.11	<i>Relative variation of the seasonal mean precipitation in DJF (a) and JJA (b) between the POLLUTED and the PRISTINE runs. Coloured pixels represent points that are significant at the 95% confidence level. Elevation contours are shown every 500 m.</i>	45
4.1	<i>Difference in seasonal mean daily temperature between WRF and the observational dataset EOBS: DJF (a), MAM (b), JJA (c) and SON (d).</i>	50
4.2	<i>Pdf of daily seasonal mean temperature of three different datasets all interpolated over the EOBS grid resolution: WRF (green line), ERA5_LAND (red line) and EOBS (blue line). DJF (a), MAM (b), JJA (c) and SON (d).</i>	51
4.3	<i>Monthly mean precipitation averaged over the GAR. Error bars represent the interannual variability of the mean monthly precipitation over the entire domain (standard deviation).</i>	52
4.4	<i>Difference in seasonal mean precipitation between WRF and the ERA5 dataset: DJF (a), MAM (b), JJA (c) and SON (d).</i>	53
4.5	<i>Probability density functions of the daily precipitation in each season. WRF is represented by the green line, ERA5 red line, and EOBS blue line.</i>	53
4.6	<i>Seasonal two meters mean temperature difference between future and historical simulation: DJF (a), MAM (b), JJA (c), and SON (d). Isolines represent the elevation every 500m.</i>	55
4.7	<i>Scatter plot of the difference in the seasonal two meters mean temperature between future and historical simulation in function of the altitude. Colors represent the density of the points in the GAR from yellow (high density) to blue (low density). Error bars represent the standard deviation calculated over each band of altitude.</i>	56
4.8	<i>Mean seasonal temperature of the future (a) and historical (b) simulations. Relative variation of the Albedo (c). All the figures represent DJF season. Isolines represent the elevation every 500m.</i>	57
4.9	<i>Relative variation of the mean annual number of days with minimum temperature below 0°C, index Frost days (a). Scatter plot of the relative variation of the frost days index in function of the altitude (b). In a) isolines represent the elevation every 500m. In b) colors represent the density of the points in the GAR from yellow (high density) to blue (low density) and error bars represent the standard deviation calculated over each band of altitude.</i>	58

4.10	<i>Relative variation of mean annual number of days with a maximum temperature greater than the 95th percentile value of the distribution of maximum temperatures observed in the historical simulation, SU95P index (a). Scatter plot of the relative variation of the SU95P index in function of the altitude (b). In a) isolines represent the elevation every 500m. In b) colors represent the density of the points in the GAR from yellow (high density) to blue (low density) and error bars represent the standard deviation calculated over each band of altitude.</i>	59
4.11	<i>Relative variation of seasonal precipitation: DJF (a), MAM (b), JJA (c), and SON (d). Isolines represent the elevation every 500m.</i>	60
4.12	<i>Relative variation of seasonal precipitation in function of the altitude: DJF (a), MAM (b), JJA (c), and SON (d). Error bars represent the standard deviation calculated over each band of altitude. Colors represent the density of the points in the GAR from yellow (high density) to blue (low density).</i>	61
4.13	<i>Maps of the relative variation of the mean seasonal number of days with daily precipitation greater than 20mm (R20 index): DJF (a), MAM (b), JJA (c), and SON (d). Isolines represent the elevation every 500m.</i>	62
4.14	<i>Relative variation of the R20 index in function of the altitude: DJF (a), MAM (b), JJA (c), and SON (d). Error bars represent the standard deviation calculated over each band of altitude. Colors represent the density of the points in the GAR from yellow (high density) to blue (low density).</i>	63
4.15	<i>Maps of the relative variation of the seasonal average of the cumulative precipitation that is above the 95th daily historical percentile on wet days ($RR \geq 1mm$) (R295pTOT index): DJF (a), MAM (b), JJA (c), and SON (d). Isolines represent the elevation every 500m.</i>	64
4.16	<i>Relative variation of the R95pTOT index in function of the altitude: DJF (a), MAM (b), JJA (c), and SON (d). Error bars represent the standard deviation calculated over each band of altitude. Colors represent the density of the points in the GAR from yellow (high density) to blue (low density).</i>	65
4.17	<i>Relative variation of the annual mean of the maximum number of consecutive days with less than 1 mm/day of rain, CDD index (a). Scatter plot of the relative variation of the SU95P index in function of the altitude (b). In a) isolines represent the elevation every 500m. In b) colors represent the density of the points in the GAR from yellow (high density) to blue (low density) and error bars represent the standard deviation calculated over each band of altitude.</i>	66
A.1	<i>ARW η coordinates [140]</i>	75

List of Tables

2.1	<i>Border latitude and longitude of the different subregions of fig. 2.10.</i>	24
2.2	<i>Number of stations for each subregion.</i>	24
2.3	<i>Correlation between time series of annual precipitation in the different regions among each others and with the mean GAR time series. All the correlations are significant at least at the 95% confidence level.</i>	26
2.4	<i>Correlation with NAO of seasonal and annual precipitations over the GAR and Lombardy region for mountains, lowlands and Ro. The correlation is calculated between detrended variables. Correlation coefficients significant at the 95% confidence level (as discussed in the section "Methods" of the main paper) are shown in bold. Correlations with GAR have been computed over the 1961-1990 period. Correlations with Lombardy region have been computed over the 1950-2016 period.</i>	28
2.5	<i>Correlation with AMO of seasonal precipitations over the GAR for mountains, lowland and Ro and over the Lombardy region for Ro. The correlation is calculated between detrended variables. None of the correlations is statistically significant. Correlations with GAR have been computed over the 1961-1990 period. Correlations with Lombardy region have been computed over the 1950-2016 period.</i>	29
4.1	<i>Mean temperature and the relative spatial standard deviation over the entire domain for the dataset WRF, ERA_LAND and EOBS.</i>	50

Bibliography

- [1] C. B. Field, V. Barros, T. F. Stocker, and Q. Dahe, *Managing the risks of extreme events and disasters to advance climate change adaptation: special report of the intergovernmental panel on climate change*. Cambridge University Press, 2012.
- [2] B. D. Santer, K. Taylor, T. Wigley, T. Johns, P. Jones, D. Karoly, J. Mitchell, A. Oort, J. Penner, V. Ramaswamy, *et al.*, “A search for human influences on the thermal structure of the atmosphere,” *Nature*, vol. 382, no. 6586, pp. 39–46, 1996.
- [3] V. Ramaswamy, M. Schwarzkopf, W. Randel, B. Santer, B. Soden, and G. Stenchikov, “Anthropogenic and natural influences in the evolution of lower stratospheric cooling,” *Science*, vol. 311, no. 5764, pp. 1138–1141, 2006.
- [4] T. Stocker, *Climate change 2013: the physical science basis: Working Group I contribution to the Fifth assessment report of the Intergovernmental Panel on Climate Change*. Cambridge university press, 2014.
- [5] V. Masson-Delmotte, P. Zhai, H. Pörtner, D. Roberts, J. Skea, P. Shukla, A. Pirani, W. Moufouma-Okia, C. Péan, R. Pidcock, *et al.*, “Ipcc, 2018: Summary for policymakers. in: Global warming of 1.5 c. an ipcc special report on the impacts of global warming of 1.5 c above pre-industrial levels and related global greenhouse gas emission pathways, in the context of strengthening the global,” *World Meteorological Organization, Geneva, Tech. Rep*, 2018.
- [6] C. Huggel, M. Carey, J. J. Clague, S. Fraser, and A. Kääb, *The high-mountain cryosphere: Environmental changes and human risks*. Cambridge University Press, 2015.
- [7] D. Viviroli, H. H. Dürr, B. Messerli, M. Meybeck, and R. Weingartner, “Mountains of the world, water towers for humanity: Typology, mapping, and global significance,” *Water resources research*, vol. 43, no. 7, 2007.
- [8] R. Hock, G. Rasul, C. Adler, B. Cáceres, S. Gruber, Y. Hirabayashi, M. Jackson, A. Kääb, S. Kang, S. Kutuzov, *et al.*, “High mountain areas supplementary material,” *IPCC Special Report on the Ocean and Cryosphere in a Changing Climate*, 2019.

- [9] J. W. Oyler, S. Z. Dobrowski, A. P. Ballantyne, A. E. Klene, and S. W. Running, “Artificial amplification of warming trends across the mountains of the western united states,” *Geophysical research letters*, vol. 42, no. 1, pp. 153–161, 2015.
- [10] R. Nitu, Y.-A. Roulet, M. Wolff, M. E. Earle, A. Reverdin, C. D. Smith, J. Kochendorfer, S. Morin, R. Rasmussen, K. Wong, *et al.*, “Wmo solid precipitation intercomparison experiment (spice)(2012-2015),” 2019.
- [11] J. H. Lawrimore, M. J. Menne, B. E. Gleason, C. N. Williams, D. B. Wuertz, R. S. Vose, and J. Rennie, “An overview of the global historical climatology network monthly mean temperature data set, version 3,” *Journal of Geophysical Research: Atmospheres*, vol. 116, no. D19, 2011.
- [12] M. Ménégou, G. Krinner, Y. Balkanski, O. Boucher, A. Cozic, S. Lim, P. Ginot, P. Laj, H. Gallée, P. Wagnon, *et al.*, “Snow cover sensitivity to black carbon deposition in the himalayas: from atmospheric and ice core measurements to regional climate simulations,” *Atmospheric Chemistry and Physics*, vol. 14, no. 8, pp. 4237–4249, 2014.
- [13] J.-P. W. Kevin, S. Kotlarski, S. C. Scherrer, and C. Schär, “The alpine snow-albedo feedback in regional climate models,” *Climate dynamics*, vol. 48, no. 3, pp. 1109–1124, 2017.
- [14] N. Pepin, R. S. Bradley, H. Diaz, M. Baraër, E. Caceres, N. Forsythe, H. Fowler, G. Greenwood, M. Hashmi, X. Liu, *et al.*, “Elevation-dependent warming in mountain regions of the world,” *Nature climate change*, vol. 5, no. 5, pp. 424–430, 2015.
- [15] H. Hartmann and L. Andresky, “Flooding in the indus river basin—a spatiotemporal analysis of precipitation records,” *Global and planetary change*, vol. 107, pp. 25–35, 2013.
- [16] J. S. Mankin and N. S. Diffenbaugh, “Influence of temperature and precipitation variability on near-term snow trends,” *Climate Dynamics*, vol. 45, no. 3, pp. 1099–1116, 2015.
- [17] X. Rodó, E. Baert, and F. Comin, “Variations in seasonal rainfall in southern europe during the present century: relationships with the north atlantic oscillation and the el niño-southern oscillation,” *Climate Dynamics*, vol. 13, no. 4, pp. 275–284, 1997.
- [18] J. W. Hurrell and H. Van Loon, “Decadal variations in climate associated with the north atlantic oscillation,” in *Climatic change at high elevation sites*, pp. 69–94, Springer, 1997.
- [19] F. Giorgi and E. Coppola, “European climate-change oscillation (eco),” *Geophysical Research Letters*, vol. 34, no. 21, 2007.
- [20] M. Zemp, H. Frey, I. Gärtner-Roer, S. U. Nussbaumer, M. Hoelzle, F. Paul, W. Haeberli, F. Denzinger, A. P. Ahlstrøm, B. Anderson, *et al.*, “Historically unprecedented global glacier decline in the early 21st century,” *Journal of glaciology*, vol. 61, no. 228, pp. 745–762, 2015.

- [21] W. G. Medwedeff and G. H. Roe, “Trends and variability in the global dataset of glacier mass balance,” *Climate dynamics*, vol. 48, no. 9-10, pp. 3085–3097, 2017.
- [22] B. Marzeion, A. Jarosch, and J. M. Gregory, “Feedbacks and mechanisms affecting the global sensitivity of glaciers to climate change,” *The Cryosphere*, vol. 8, no. 1, pp. 59–71, 2014.
- [23] M. Vuille, M. Carey, C. Huggel, W. Buytaert, A. Rabatel, D. Jacobsen, A. Soruco, M. Villacis, C. Yarleque, O. E. Timm, *et al.*, “Rapid decline of snow and ice in the tropical andes—impacts, uncertainties and challenges ahead,” *Earth-Science Reviews*, vol. 176, pp. 195–213, 2018.
- [24] Y. Hirabayashi, K. Nakano, Y. Zhang, S. Watanabe, M. Tanoue, and S. Kanae, “Contributions of natural and anthropogenic radiative forcing to mass loss of northern hemisphere mountain glaciers and quantifying their uncertainties,” *Scientific reports*, vol. 6, no. 1, pp. 1–7, 2016.
- [25] R. L. Armstrong and E. Brun, *Snow and climate: physical processes, surface energy exchange and modeling*. Cambridge University Press, 2008.
- [26] Q. You, A. Sanchez-Lorenzo, M. Wild, D. Folini, K. Fraedrich, G. Ren, and S. Kang, “Decadal variation of surface solar radiation in the tibetan plateau from observations, re-analysis and model simulations,” *Climate dynamics*, vol. 40, no. 7, pp. 2073–2086, 2013.
- [27] M. Beniston, D. Farinotti, M. Stoffel, L. M. Andreassen, E. Coppola, N. Eckert, A. Fantini, F. Giacona, C. Hauck, M. Huss, *et al.*, “The european mountain cryosphere: a review of its current state, trends, and future challenges,” *The Cryosphere*, vol. 12, no. 2, pp. 759–794, 2018.
- [28] J. R. Minder, T. W. Letcher, and C. Liu, “The character and causes of elevation-dependent warming in high-resolution simulations of rocky mountain climate change,” *Journal of Climate*, vol. 31, no. 6, pp. 2093–2113, 2018.
- [29] E. Palazzi, L. Mortarini, S. Terzago, and J. Von Hardenberg, “Elevation-dependent warming in global climate model simulations at high spatial resolution,” *Climate Dynamics*, vol. 52, no. 5, pp. 2685–2702, 2019.
- [30] I. Rangwala, E. Sinsky, and J. R. Miller, “Amplified warming projections for high altitude regions of the northern hemisphere mid-latitudes from cmip5 models,” *Environmental Research Letters*, vol. 8, no. 2, p. 024040, 2013.
- [31] Y. Chen, C. M. Naud, I. Rangwala, C. C. Landry, and J. R. Miller, “Comparison of the sensitivity of surface downward longwave radiation to changes in water vapor at two high elevation sites,” *Environmental Research Letters*, vol. 9, no. 11, p. 114015, 2014.

- [32] A. Ohmura, “Enhanced temperature variability in high-altitude climate change,” *Theoretical and Applied Climatology*, vol. 110, no. 4, pp. 499–508, 2012.
- [33] N. Pepin and J. Lundquist, “Temperature trends at high elevations: patterns across the globe,” *Geophysical Research Letters*, vol. 35, no. 14, 2008.
- [34] S. Scherrer, P. Ceppi, M. Croci-Maspoli, and C. Appenzeller, “Snow-albedo feedback and swiss spring temperature trends,” *Theoretical and Applied Climatology*, vol. 110, no. 4, pp. 509–516, 2012.
- [35] Z. Zeng, A. Chen, P. Ciais, Y. Li, L. Z. Li, R. Vautard, L. Zhou, H. Yang, M. Huang, and S. Piao, “Regional air pollution brightening reverses the greenhouse gases induced warming-elevation relationship,” *Geophysical Research Letters*, vol. 42, no. 11, pp. 4563–4572, 2015.
- [36] I. M. Held and B. J. Soden, “Robust responses of the hydrological cycle to global warming,” *Journal of climate*, vol. 19, no. 21, pp. 5686–5699, 2006.
- [37] A. Bigi, G. Ghermandi, and R. M. Harrison, “Analysis of the air pollution climate at a background site in the po valley,” *Journal of Environmental Monitoring*, vol. 14, no. 2, pp. 552–563, 2012.
- [38] A. Bigi and G. Ghermandi, “Long-term trend and variability of atmospheric pm 10 concentration in the po valley,” *Atmospheric Chemistry and Physics*, vol. 14, no. 10, pp. 4895–4907, 2014.
- [39] S. Fuzzi, U. Baltensperger, K. Carslaw, S. Decesari, H. Denier van der Gon, M. C. Facchini, D. Fowler, I. Koren, B. Langford, U. Lohmann, *et al.*, “Particulate matter, air quality and climate: lessons learned and future needs,” *Atmospheric chemistry and physics*, vol. 15, no. 14, pp. 8217–8299, 2015.
- [40] G. Guariso and M. Volta, “Air quality in europe: Today and tomorrow,” in *Air Quality Integrated Assessment*, pp. 1–8, Springer, Cham, 2017.
- [41] I. Auer, R. Böhm, A. Jurkovic, W. Lipa, A. Orlik, R. Potzmann, W. Schöner, M. Ungersböck, C. Matulla, K. Briffa, *et al.*, “Himalp—historical instrumental climatological surface time series of the greater alpine region,” *International Journal of Climatology: A Journal of the Royal Meteorological Society*, vol. 27, no. 1, pp. 17–46, 2007.
- [42] P. Ceppi, S. C. Scherrer, A. M. Fischer, and C. Appenzeller, “Revisiting swiss temperature trends 1959–2008,” *International Journal of Climatology*, vol. 32, no. 2, pp. 203–213, 2012.

- [43] H. Zekollari, M. Huss, and D. Farinotti, “Modelling the future evolution of glaciers in the european alps under the euro-cordex rcm ensemble,” *The Cryosphere*, vol. 13, no. 4, pp. 1125–1146, 2019.
- [44] M. Žebre, R. R. Colucci, F. Giorgi, N. F. Glasser, A. E. Racoviteanu, and C. Del Gobbo, “200 years of equilibrium-line altitude variability across the european alps (1901- 2100),” *Climate Dynamics*, vol. 56, no. 3, pp. 1183–1201, 2021.
- [45] I. Auer and R. Böhm, “Combined temperature-precipitation variations in austria during the instrumental period,” *Theoretical and applied climatology*, vol. 49, no. 3, pp. 161–174, 1994.
- [46] J.-F. Rysman, Y. Lemaître, and E. Moreau, “Spatial and temporal variability of rainfall in the alps–mediterranean euroregion,” *Journal of Applied Meteorology and Climatology*, vol. 55, no. 3, pp. 655–671, 2016.
- [47] A. B. Pieri, J. von Hardenberg, A. Parodi, and A. Provenzale, “Sensitivity of precipitation statistics to resolution, microphysics, and convective parameterization: A case study with the high-resolution wrf climate model over europe,” *Journal of Hydrometeorology*, vol. 16, no. 4, pp. 1857–1872, 2015.
- [48] N. Ban, C. Caillaud, E. Coppola, E. Pichelli, S. Sobolowski, M. Adinolfi, B. Ahrens, A. Alias, I. Anders, S. Bastin, *et al.*, “The first multi-model ensemble of regional climate simulations at kilometer-scale resolution, part i: evaluation of precipitation,” *Climate Dynamics*, pp. 1–28, 2021.
- [49] E. Pichelli, E. Coppola, S. Sobolowski, N. Ban, F. Giorgi, P. Stocchi, A. Alias, D. Belušić, S. Berthou, C. Caillaud, *et al.*, “The first multi-model ensemble of regional climate simulations at kilometer-scale resolution part 2: historical and future simulations of precipitation,” *Climate Dynamics*, vol. 56, no. 11, pp. 3581–3602, 2021.
- [50] F. Giorgi, C. Torma, E. Coppola, N. Ban, C. Schär, and S. Somot, “Enhanced summer convective rainfall at alpine high elevations in response to climate warming,” *Nature Geoscience*, vol. 9, no. 8, pp. 584–589, 2016.
- [51] E. Dallan, M. Borga, M. Zaramella, and F. Marra, “Enhanced summer convection explains observed trends in extreme subdaily precipitation in the northeastern italian alps,” 2021.
- [52] J. Haywood and K. Shine, “The effect of anthropogenic sulfate and soot aerosol on the clear sky planetary radiation budget,” *Geophysical Research Letters*, vol. 22, no. 5, pp. 603–606, 1995.
- [53] B. A. Albrecht, “Aerosols, cloud microphysics, and fractional cloudiness,” *Science*, vol. 245, no. 4923, pp. 1227–1230, 1989.

- [54] V. Ramanathan, P. Crutzen, J. Kiehl, and D. Rosenfeld, “Aerosols, climate, and the hydrological cycle,” *science*, vol. 294, no. 5549, pp. 2119–2124, 2001.
- [55] D. Rosenfeld, U. Lohmann, G. B. Raga, C. D. O’Dowd, M. Kulmala, S. Fuzzi, A. Reissell, and M. O. Andreae, “Flood or drought: How do aerosols affect precipitation?,” *science*, vol. 321, no. 5894, pp. 1309–1313, 2008.
- [56] J. Hansen, M. Sato, and R. Ruedy, “Radiative forcing and climate response,” *Journal of Geophysical Research: Atmospheres*, vol. 102, no. D6, pp. 6831–6864, 1997.
- [57] J. E. Penner, M. Andreae, H. Annegarn, L. Barrie, J. Feichter, D. Hegg, A. Jayaraman, R. Leaitch, D. Murphy, J. Nganga, *et al.*, “Aerosols, their direct and indirect effects,” in *Climate Change 2001: The Scientific Basis. Contribution of Working Group I to the Third Assessment Report of the Intergovernmental Panel on Climate Change*, pp. 289–348, Cambridge University Press, 2001.
- [58] S. Zhang, M. Wang, S. J. Ghan, A. Ding, H. Wang, K. Zhang, D. Neubauer, U. Lohmann, S. Ferrachat, T. Takeamura, *et al.*, “On the characteristics of aerosol indirect effect based on dynamic regimes in global climate models,” *Atmospheric Chemistry and Physics*, vol. 16, no. 5, pp. 2765–2783, 2016.
- [59] S. Solomon, M. Manning, M. Marquis, D. Qin, *et al.*, *Climate change 2007-the physical science basis: Working group I contribution to the fourth assessment report of the IPCC*, vol. 4. Cambridge university press, 2007.
- [60] O. Edenhofer, *Climate change 2014: mitigation of climate change*, vol. 3. Cambridge University Press, 2015.
- [61] A. Givati and D. Rosenfeld, “Quantifying precipitation suppression due to air pollution,” *Journal of Applied meteorology*, vol. 43, no. 7, pp. 1038–1056, 2004.
- [62] I. L. Jirak and W. R. Cotton, “Effect of air pollution on precipitation along the front range of the rocky mountains,” *Journal of Applied Meteorology and Climatology*, vol. 45, no. 1, pp. 236–245, 2006.
- [63] B. Lynn, A. Khain, D. Rosenfeld, and W. L. Woodley, “Effects of aerosols on precipitation from orographic clouds,” *Journal of Geophysical Research: Atmospheres*, vol. 112, no. D10, 2007.
- [64] P. Alpert, N. Halfon, and Z. Levin, “Does air pollution really suppress precipitation in israel?,” *Journal of Applied Meteorology and Climatology*, vol. 47, no. 4, pp. 933–943, 2008.

- [65] N. Siler and G. Roe, “How will orographic precipitation respond to surface warming? an idealized thermodynamic perspective,” *Geophysical Research Letters*, vol. 41, no. 7, pp. 2606–2613, 2014.
- [66] X. Shi and D. R. Durran, “The response of orographic precipitation over idealized mid-latitude mountains due to global increases in co₂,” *Journal of Climate*, vol. 27, no. 11, pp. 3938–3956, 2014.
- [67] A. Crespi, M. Brunetti, G. Lentini, and M. Maugeri, “1961–1990 high-resolution monthly precipitation climatologies for italy,” *International Journal of Climatology*, vol. 38, no. 2, pp. 878–895, 2018.
- [68] M. Brunetti, M. Maugeri, F. Monti, and T. Nanni, “Temperature and precipitation variability in italy in the last two centuries from homogenised instrumental time series,” *International Journal of Climatology: A Journal of the Royal Meteorological Society*, vol. 26, no. 3, pp. 345–381, 2006.
- [69] C. S. Bretherton, M. Widmann, V. P. Dymnikov, J. M. Wallace, and I. Bladé, “The effective number of spatial degrees of freedom of a time-varying field,” *Journal of climate*, vol. 12, no. 7, pp. 1990–2009, 1999.
- [70] C. Frei and C. Schär, “A precipitation climatology of the alps from high-resolution rain-gauge observations,” *International Journal of Climatology: A Journal of the Royal Meteorological Society*, vol. 18, no. 8, pp. 873–900, 1998.
- [71] F. A. Isotta, C. Frei, V. Weilguni, M. Perčec Tadić, P. Lassegues, B. Rudolf, V. Pavan, C. Cacciamani, G. Antolini, S. M. Ratto, *et al.*, “The climate of daily precipitation in the alps: development and analysis of a high-resolution grid dataset from pan-alpine rain-gauge data,” *International Journal of Climatology*, vol. 34, no. 5, pp. 1657–1675, 2014.
- [72] J. W. Hurrell and C. Deser, “North atlantic climate variability: the role of the north atlantic oscillation,” *Journal of marine systems*, vol. 79, no. 3-4, pp. 231–244, 2010.
- [73] Y. Brugnara and M. Maugeri, “Daily precipitation variability in the southern alps since the late 19th century,” *International journal of climatology*, vol. 39, no. 8, pp. 3492–3504, 2019.
- [74] C. H. O’Reilly, T. Woollings, and L. Zanna, “The dynamical influence of the atlantic multidecadal oscillation on continental climate,” *Journal of Climate*, vol. 30, no. 18, pp. 7213–7230, 2017.
- [75] M. Zampieri, A. Toreti, A. Schindler, E. Scoccimarro, and S. Gualdi, “Atlantic multidecadal oscillation influence on weather regimes over europe and the mediterranean in spring and summer,” *Global and Planetary Change*, vol. 151, pp. 92–100, 2017.

- [76] J. W. Hurrell, “Decadal trends in the north atlantic oscillation: Regional temperatures and precipitation,” *Science*, vol. 269, no. 5224, pp. 676–679, 1995.
- [77] B. Qian, J. Corte-Real, and H. Xu, “Is the north atlantic oscillation the most important atmospheric pattern for precipitation in europe?,” *Journal of Geophysical Research: Atmospheres*, vol. 105, no. D9, pp. 11901–11910, 2000.
- [78] G. Stefanicki, P. Talkner, and R. Weber, “Frequency changes of weather types in the alpine region since 1945,” *Theoretical and Applied Climatology*, vol. 60, no. 1, pp. 47–61, 1998.
- [79] M. Schwander, S. Brönnimann, G. Delaygue, M. Rohrer, R. Auchmann, and Y. Brugnara, “Reconstruction of central european daily weather types back to 1763,” *International journal of climatology*, vol. 37, pp. 30–44, 2017.
- [80] M. P. Clark, R. L. Wilby, E. D. Gutmann, J. A. Vano, S. Gangopadhyay, A. W. Wood, H. J. Fowler, C. Prudhomme, J. R. Arnold, and L. D. Brekke, “Characterizing uncertainty of the hydrologic impacts of climate change,” *Current Climate Change Reports*, vol. 2, no. 2, pp. 55–64, 2016.
- [81] V. Manara, M. Brunetti, A. Celozzi, M. Maugeri, A. Sanchez-Lorenzo, and M. Wild, “Detection of dimming/brightening in italy from homogenized all-sky and clear-sky surface solar radiation records and underlying causes (1959–2013),” *Atmospheric Chemistry and Physics*, vol. 16, no. 17, pp. 11145–11161, 2016.
- [82] M. Tudoroiu, E. Eccel, B. Gioli, D. Gianelle, H. Schume, L. Genesio, and F. Miglietta, “Negative elevation-dependent warming trend in the eastern alps,” *Environmental Research Letters*, vol. 11, no. 4, p. 044021, 2016.
- [83] V. Manara, M. Bassi, M. Brunetti, B. Cagnazzi, and M. Maugeri, “1990–2016 surface solar radiation variability and trend over the piedmont region (northwest italy),” *Theoretical and Applied Climatology*, vol. 136, no. 3, pp. 849–862, 2019.
- [84] B. Arvani, R. Pierce, A. I. Lyapustin, Y. Wang, G. Ghermandi, and S. Teggi, “High spatial resolution aerosol retrievals used for daily particulate matter monitoring over po valley, northern italy,” *Atmospheric Chemistry and Physics Discussions*, vol. 15, no. 1, pp. 123–155, 2015.
- [85] S. A. Twomey, M. Piepgrass, and T. Wolfe, “An assessment of the impact of pollution on global cloud albedo,” *Tellus B*, vol. 36, no. 5, pp. 356–366, 1984.
- [86] H. Xiao, Y. Yin, L. Jin, Q. Chen, and J. Chen, “Simulation of aerosol effects on orographic clouds and precipitation using wrf model with a detailed bin microphysics scheme,” *Atmospheric Science Letters*, vol. 15, no. 2, pp. 134–139, 2014.

- [87] A. Muhlbauer and U. Lohmann, “Sensitivity studies of aerosol–cloud interactions in mixed-phase orographic precipitation,” *Journal of Atmospheric Sciences*, vol. 66, no. 9, pp. 2517–2538, 2009.
- [88] H. Xiao, Y. Yin, L. Jin, Q. Chen, and J. Chen, “Simulation of the effects of aerosol on mixed-phase orographic clouds using the wrf model with a detailed bin microphysics scheme,” *Journal of Geophysical Research: Atmospheres*, vol. 120, no. 16, pp. 8345–8358, 2015.
- [89] J. Fan, R. Zhang, G. Li, and W.-K. Tao, “Effects of aerosols and relative humidity on cumulus clouds,” *Journal of Geophysical Research: Atmospheres*, vol. 112, no. D14, 2007.
- [90] P. Schroeder, C. Belis, J. Schnelle-Kreis, R. Herzig, A. S. Prévôt, M. Raveton, M. Kirchner, and M. Catinon, “Why air quality in the alps remains a matter of concern. the impact of organic pollutants in the alpine area,” *Environmental Science and Pollution Research*, vol. 21, no. 1, pp. 252–267, 2014.
- [91] S. Sandrini, S. Fuzzi, A. Piazzalunga, P. Prati, P. Bonasoni, F. Cavalli, M. C. Bove, M. Calvello, D. Cappelletti, C. Colombi, *et al.*, “Spatial and seasonal variability of carbonaceous aerosol across italy,” *Atmospheric Environment*, vol. 99, pp. 587–598, 2014.
- [92] I. Rangwala, J. R. Miller, G. L. Russell, and M. Xu, “Using a global climate model to evaluate the influences of water vapor, snow cover and atmospheric aerosol on warming in the tibetan plateau during the twenty-first century,” *Climate Dynamics*, vol. 34, no. 6, pp. 859–872, 2010.
- [93] C. W. Stjern, B. H. Samset, O. Boucher, T. Iversen, J.-F. Lamarque, G. Myhre, D. Shindell, and T. Takemura, “How aerosols and greenhouse gases influence the diurnal temperature range,” *Atmospheric Chemistry and Physics*, vol. 20, no. 21, pp. 13467–13480, 2020.
- [94] L. Zhang, T.-M. Fu, H. Tian, Y. Ma, J.-P. Chen, T.-C. Tsai, I.-C. Tsai, Z. Meng, and X. Yang, “Anthropogenic aerosols significantly reduce mesoscale convective system occurrences and precipitation over southern china in april,” *Geophysical Research Letters*, vol. 47, no. 6, p. e2019GL086204, 2020.
- [95] W.-K. Tao, J.-P. Chen, Z. Li, C. Wang, and C. Zhang, “Impact of aerosols on convective clouds and precipitation,” *Reviews of Geophysics*, vol. 50, no. 2, 2012.
- [96] E. Fiori, A. Comellas, L. Molini, N. Rebora, F. Siccardi, D. Gochis, S. Tanelli, and A. Parodi, “Analysis and hindcast simulations of an extreme rainfall event in the mediterranean area: The genoa 2011 case,” *Atmospheric Research*, vol. 138, pp. 13–29, 2014.
- [97] G. Thompson and T. Eidhammer, “A study of aerosol impacts on clouds and precipitation development in a large winter cyclone,” *Journal of the atmospheric sciences*, vol. 71, no. 10, pp. 3636–3658, 2014.

- [98] C. A. Ochoa, A. I. Quintanar, G. B. Raga, and D. Baumgardner, “Changes in intense precipitation events in Mexico City,” *Journal of Hydrometeorology*, vol. 16, no. 4, pp. 1804–1820, 2015.
- [99] Y. Qian, D. Gong, J. Fan, L. R. Leung, R. Bennartz, D. Chen, and W. Wang, “Heavy pollution suppresses light rain in China: Observations and modeling,” *Journal of Geophysical Research: Atmospheres*, vol. 114, no. D7, 2009.
- [100] O. Alizadeh-Choobari and M. Gharaylou, “Aerosol impacts on radiative and microphysical properties of clouds and precipitation formation,” *Atmospheric Research*, vol. 185, pp. 53–64, 2017.
- [101] O. Alizadeh-Choobari, “Impact of aerosol number concentration on precipitation under different precipitation rates,” *Meteorological Applications*, vol. 25, no. 4, pp. 596–605, 2018.
- [102] Z. Li, F. Niu, J. Fan, Y. Liu, D. Rosenfeld, and Y. Ding, “Long-term impacts of aerosols on the vertical development of clouds and precipitation,” *Nature Geoscience*, vol. 4, no. 12, pp. 888–894, 2011.
- [103] V. Pavlidis, E. Katragkou, A. Prein, A. K. Georgoulas, S. Kartsios, P. Zanis, and T. Karacostas, “Investigating the sensitivity to resolving aerosol interactions in downscaling regional model experiments with wrfv3. 8.1 over Europe,” *Geoscientific Model Development*, vol. 13, no. 6, pp. 2511–2532, 2020.
- [104] P. Davini, J. v. Hardenberg, S. Corti, H. M. Christensen, S. Juricke, A. Subramanian, P. A. Watson, A. Weisheimer, and T. N. Palmer, “Climate sphinx: evaluating the impact of resolution and stochastic physics parameterisations in the EC-Earth global climate model,” *Geoscientific Model Development*, vol. 10, no. 3, pp. 1383–1402, 2017.
- [105] M. Adinolfi, M. Raffa, A. Reder, and P. Mercogliano, “Evaluation and expected changes of summer precipitation at convection permitting scale with cosmo-clm over alpine space,” *Atmosphere*, vol. 12, no. 1, p. 54, 2021.
- [106] I. Takayabu, R. Rasmussen, E. Nakakita, A. Prein, H. Kawase, S.-I. Watanabe, S. A. Adachi, T. Takemi, K. Yamaguchi, Y. Osakada, *et al.*, “Convection-permitting models for climate research,” *Bulletin of the American Meteorological Society*, vol. 103, no. 1, pp. E77–E82, 2022.
- [107] S.-Y. Hong, Y. Noh, and J. Dudhia, “A new vertical diffusion package with an explicit treatment of entrainment processes,” *Monthly Weather Review*, vol. 134, no. 9, pp. 2318–2341, 2006.

- [108] M. J. Iacono, J. S. Delamere, E. J. Mlawer, M. W. Shephard, S. A. Clough, and W. D. Collins, “Radiative forcing by long-lived greenhouse gases: Calculations with the aer radiative transfer models,” *Journal of Geophysical Research: Atmospheres*, vol. 113, no. D13, 2008.
- [109] M. Tiedtke, “A comprehensive mass flux scheme for cumulus parameterization in large-scale models,” *Monthly weather review*, vol. 117, no. 8, pp. 1779–1800, 1989.
- [110] N. Da Silva, S. Mailler, and P. Drobinski, “Aerosol indirect effects on summer precipitation in a regional climate model for the euro-mediterranean region,” in *Annales Geophysicae*, vol. 36, pp. 321–335, 2018.
- [111] R. Van Dingenen, F. Raes, J.-P. Putaud, U. Baltensperger, A. Charron, M.-C. Facchini, S. Decesari, S. Fuzzi, R. Gehrig, H.-C. Hansson, *et al.*, “A european aerosol phenomenology—1: physical characteristics of particulate matter at kerbside, urban, rural and background sites in europe,” *Atmospheric Environment*, vol. 38, no. 16, pp. 2561–2577, 2004.
- [112] M. W. Christensen, W. K. Jones, and P. Stier, “Aerosols enhance cloud lifetime and brightness along the stratus-to-cumulus transition,” *Proceedings of the National Academy of Sciences*, vol. 117, no. 30, pp. 17591–17598, 2020.
- [113] X. Zeng, W.-K. Tao, M. Zhang, A. Y. Hou, S. Xie, S. Lang, X. Li, D. O. Starr, X. Li, and J. Simpson, “An indirect effect of ice nuclei on atmospheric radiation,” *Journal of the atmospheric sciences*, vol. 66, no. 1, pp. 41–61, 2009.
- [114] X. Zeng, W.-K. Tao, M. Zhang, A. Y. Hou, S. Xie, S. Lang, X. Li, D. O. Starr, and X. Li, “A contribution by ice nuclei to global warming,” *Quarterly Journal of the Royal Meteorological Society: A journal of the atmospheric sciences, applied meteorology and physical oceanography*, vol. 135, no. 643, pp. 1614–1629, 2009.
- [115] X. Deng, H. Xue, and Z. Meng, “The effect of ice nuclei on a deep convective cloud in south china,” *Atmospheric Research*, vol. 206, pp. 1–12, 2018.
- [116] Y. Yang, J. Sun, Y. Zhu, and T. Zhang, “Examination of the impacts of ice nuclei aerosol particles on microphysics, precipitation and electrification in a 1.5d aerosol-cloud bin model,” *Journal of Aerosol Science*, vol. 140, p. 105440, 2020.
- [117] H. Jiang, H. Xue, A. Teller, G. Feingold, and Z. Levin, “Aerosol effects on the lifetime of shallow cumulus,” *Geophysical Research Letters*, vol. 33, no. 14, 2006.
- [118] J. D. Small, P. Y. Chuang, G. Feingold, and H. Jiang, “Can aerosol decrease cloud lifetime?,” *Geophysical Research Letters*, vol. 36, no. 16, 2009.

- [119] E. Palazzi, L. Filippi, and J. von Hardenberg, “Insights into elevation-dependent warming in the tibetan plateau-himalayas from cmip5 model simulations,” *Climate Dynamics*, vol. 48, no. 11, pp. 3991–4008, 2017.
- [120] M. Haylock, N. Hofstra, A. Klein Tank, E. Klok, P. Jones, and M. New, “A european daily high-resolution gridded data set of surface temperature and precipitation for 1950–2006,” *Journal of Geophysical Research: Atmospheres*, vol. 113, no. D20, 2008.
- [121] R. C. Cornes, G. van der Schrier, E. J. van den Besselaar, and P. D. Jones, “An ensemble version of the e-obs temperature and precipitation data sets,” *Journal of Geophysical Research: Atmospheres*, vol. 123, no. 17, pp. 9391–9409, 2018.
- [122] N. Hofstra, M. Haylock, M. New, and P. D. Jones, “Testing e-obs european high-resolution gridded data set of daily precipitation and surface temperature,” *Journal of Geophysical Research: Atmospheres*, vol. 114, no. D21, 2009.
- [123] J. Muñoz-Sabater, E. Dutra, A. Agustí-Panareda, C. Albergel, G. Arduini, G. Balsamo, S. Boussetta, M. Choulga, S. Harrigan, H. Hersbach, *et al.*, “Era5-land: A state-of-the-art global reanalysis dataset for land applications,” *Earth System Science Data Discussions*, pp. 1–50, 2021.
- [124] H. Hersbach, B. Bell, P. Berrisford, S. Hirahara, A. Horányi, J. Muñoz-Sabater, J. Nicolas, C. Peubey, R. Radu, D. Schepers, *et al.*, “The era5 global reanalysis,” *Quarterly Journal of the Royal Meteorological Society*, vol. 146, no. 730, pp. 1999–2049, 2020.
- [125] P. W. Jones, “First-and second-order conservative remapping schemes for grids in spherical coordinates,” *Monthly Weather Review*, vol. 127, no. 9, pp. 2204–2210, 1999.
- [126] G. Smiatek, H. Kunstmann, and A. Senatore, “Euro-cordex regional climate model analysis for the greater alpine region: Performance and expected future change,” *Journal of Geophysical Research: Atmospheres*, vol. 121, no. 13, pp. 7710–7728, 2016.
- [127] S. Kotlarski, K. Keuler, O. B. Christensen, A. Colette, M. Déqué, A. Gobiet, K. Goergen, D. Jacob, D. Lüthi, E. Van Meijgaard, *et al.*, “Regional climate modeling on european scales: a joint standard evaluation of the euro-cordex rcm ensemble,” *Geoscientific Model Development*, vol. 7, no. 4, pp. 1297–1333, 2014.
- [128] T. R. Karl, N. Nicholls, and A. Ghazi, “Clivar/gcos/wmo workshop on indices and indicators for climate extremes workshop summary,” in *Weather and climate extremes*, pp. 3–7, Springer, 1999.
- [129] T. Peterson, C. Folland, G. Gruza, W. Hogg, A. Mokssit, and N. Plummer, *Report on the activities of the working group on climate change detection and related rapporteurs*. Citeseer, 2001.

- [130] P. Frei, S. Kotlarski, M. A. Liniger, and C. Schär, “Future snowfall in the alps: projections based on the euro-cordex regional climate models,” *The Cryosphere*, vol. 12, no. 1, pp. 1–24, 2018.
- [131] S. Russo, J. Sillmann, and E. M. Fischer, “Top ten european heatwaves since 1950 and their occurrence in the coming decades,” *Environmental Research Letters*, vol. 10, no. 12, p. 124003, 2015.
- [132] E. Kjellström, G. Nikulin, G. Strandberg, O. B. Christensen, D. Jacob, K. Keuler, G. Lenderink, E. van Meijgaard, C. Schär, S. Somot, *et al.*, “European climate change at global mean temperature increases of 1.5 and 2 c above pre-industrial conditions as simulated by the euro-cordex regional climate models,” *Earth System Dynamics*, vol. 9, no. 2, pp. 459–478, 2018.
- [133] G. Heinrich and A. Gobiet, “The future of dry and wet spells in europe: a comprehensive study based on the ensembles regional climate models,” *International Journal of Climatology*, vol. 32, no. 13, pp. 1951–1970, 2012.
- [134] E. Coppola, R. Nogherotto, J. M. Ciarlo’, F. Giorgi, E. van Meijgaard, N. Kadyrov, C. Iles, L. Corre, M. Sandstad, S. Somot, *et al.*, “Assessment of the european climate projections as simulated by the large euro-cordex regional and global climate model ensemble,” *Journal of Geophysical Research: Atmospheres*, vol. 126, no. 4, p. e2019JD032356, 2021.
- [135] D. Jacob, J. Petersen, B. Eggert, A. Alias, O. B. Christensen, L. M. Bouwer, A. Braun, A. Colette, M. Déqué, G. Georgievski, *et al.*, “Euro-cordex: new high-resolution climate change projections for european impact research,” *Regional environmental change*, vol. 14, no. 2, pp. 563–578, 2014.
- [136] J. Rajczak and C. Schär, “Projections of future precipitation extremes over europe: A multimodel assessment of climate simulations,” *Journal of Geophysical Research: Atmospheres*, vol. 122, no. 20, pp. 10–773, 2017.
- [137] Y. Trambly and S. Somot, “Future evolution of extreme precipitation in the mediterranean,” *Climatic Change*, vol. 151, no. 2, pp. 289–302, 2018.
- [138] E. Moreno-Chamarro, L.-P. Caron, P. Ortega, S. L. Tomas, and M. J. Roberts, “Can we trust cmip5/6 future projections of european winter precipitation?,” *Environmental Research Letters*, vol. 16, no. 5, p. 054063, 2021.
- [139] R. Laprise, “The euler equations of motion with hydrostatic pressure as an independent variable,” *Monthly weather review*, vol. 120, no. 1, pp. 197–207, 1992.

- [140] W. C. Skamarock, J. B. Klemp, J. Dudhia, D. O. Gill, D. M. Barker, W. Wang, and J. G. Powers, “A description of the advanced research wrf version 3. near technical note-475+str,” 2008.
- [141] G. K. Vallis, *Atmospheric and oceanic fluid dynamics*. Cambridge University Press, 2017.
- [142] W. Wang and N. L. Seaman, “A comparison study of convective parameterization schemes in a mesoscale model,” *Monthly Weather Review*, vol. 125, no. 2, pp. 252–278, 1997.